Bistability in dissipatively coupled cavity magnonics

H. Pan [1,2,*], Y. Yang [2], Z. H. An [1,3,4,†] and C.-M. Hu [2,‡]

[1]*State Key Laboratory of Surface Physics, Department of Physics, Fudan University, Shanghai 200433, People's Republic of China*
[2]*Department of Physics and Astronomy, University of Manitoba, Winnipeg, Canada R3T 2N2*
[3]*Institute of Nanoelectronic Devices and Quantum Computing, Fudan University, Shanghai 200433, People's Republic of China*
[4]*Shanghai Qi Zhi Institute, Xuhui District, Shanghai 200232, People's Republic of China*

Dissipative coupling of resonators arising from their cooperative dampings to a common reservoir induces intriguingly new physics such as energy level attraction. In this study, we report the nonlinear properties in a dissipatively coupled cavity magnonic system. A magnetic material yttrium iron garnet is placed at the magnetic field node of a Fabry-Perot-like microwave cavity such that the magnons and cavity photons are dissipatively coupled. Under high power excitation, a nonlinear effect is observed in the transmission spectra, showing bistable behaviors. The observed bistabilities are manifested as clockwise, counterclockwise, and butterfly-like hysteresis loops with different frequency detuning. The experimental results are well explained as a Duffing oscillator dissipatively coupled with a harmonic one and the required trigger condition for bistability could be determined quantitatively by the coupled oscillator model. Our results demonstrate that the magnon damping has been suppressed by the dissipative interaction, which thereby reduces the threshold for conventional magnon Kerr bistability. This work sheds light on potential applications in developing low power nonlinearity devices, enhanced anharmonicity sensors and for exploring the non-Hermitian physics of cavity magnonics in the nonlinear regime.

I. INTRODUCTION

Nonlinearities are ubiquitous phenomena in various physics fields. For instance, Kerr nonlinearity and resonant two-level nonlinearity [1], leading to anharmonicities, have been widely investigated in the context of optics [2]. One signature of nonlinear dynamics is bistability for a given input exceeding a threshold power and manifests itself as a foldover effect [3–7]. The effects of nonlinearity have technological implications in sophisticated optical devices for controlling light with light [8], novel memory devices based on magnetic nonlinearity [9,10] or photonic nonlinearity [11–13], switches with bistable metamaterial [14], as well as developed mechanical devices for emergent applications like energy harvesting [15,16].

Hybrid quantum systems, which have aroused tremendous interest for application in quantum information processing [17,18], have the potential to push the development of the realm of nonlinearity. Among various hybrid subsystems, cavity magnonics [19] appears to be an exceptional candidate (see, e.g., Refs. [20–35]), which utilizes ferrimagnetic materials like yttrium iron garnet (YIG) to create collective spin excitations. This cavity magnonics system has resulted in a variety of semiclassical and quantum phenomena including, cavity-magnon polaritons [36–38], magnon bistability [34,39,40], bidirectional microwave-optical conversion mediated by ferromagnetic magnons [41], magnon dark mode [24], synchronization via spin-photon coupling [42], and non-Hermitian exotic properties [30,43,44]. In light of the well reported nonlinearities in uncoupled magnetic system during last decades [4–6,45,46], recent work has attempted to utilize the photon-magnon coupling freedom to tune the nonlinearity. The magnon-polariton bistability has been successfully observed in a coherent hybrid system [34] and the bistable behavior could also be directly measured with the coupled cavity being pumped [40]. However, in these reported works the photon-magnon are typically coherently coupled, and their coherent coupling enhances the damping of magnon states [47]. Due to the cubic dependence of the threshold for nonlinearity on the effective damping of magnon [40], the coherent coupling of cavity-magnon hybrid system therefore increases the nonlinearity threshold which may impede the device application of nonlinearity.

Coherent coupling originates from the direct spatial overlap between photon and magnon modes and forms hybrid states with repulsed energy levels and attracted damping rates. In contrast, a dissipative form of magnon-photon interaction [48] requires no direct mode overlap and has been demonstrated to cause level attraction and a damping repulsion effect [49–51]. This dissipative coupling is indirect as it is mediated through a shared reservoir, resulting in an imaginary spin-photon coupling strength. Dissipatively coupled systems have important applications such as nonreciprocal transport [52], enhanced sensing [53], and non-Hermitian singularities [54,55]. So far, however, reported work with dissipative

*hpan19@fudan.edu.cn
†anzhenghua@fudan.edu.cn
‡hu@physics.umanitoba.ca

coupling have been focused on the linear regime and the nonlinearity with dissipative coupling have not been experimentally examined, except a theoretical prediction of a lower threshold if the (imaginary) coupling strength is sufficiently large in an anti-PT regime [56].

Inspired by this, we study a dissipatively coupled cavity-magnon system where a YIG sphere is imbedded in a Fabry-Perot-like cavity. The coupled system is directly pumped through the cavity and the pumping power is sufficiently high to create the nonlinear effect. We experimentally demonstrate that, in the dissipatively coupled nonlinear system, the threshold power for bistability is lower than the corresponding bound in coherent scenario. This is due to the suppression of magnon damping on-resonance induced by dissipative coupling. In addition, such a dissipatively coupled hybridized system results in different magnetic field and power dependent bistable behaviors as the magnon frequency is detuned for on and off cavity resonant frequency. By introducing the model based on a Duffing oscillator dissipatively coupled with a harmonic oscillator, the experimental results can be well explained. This method allows us to determine the required experimental condition for triggering bistable behavior in a dissipatively coupled system. Our work shows that dissipative coupling in a hybrid system with a nonlinear effect may be utilized to engineer a lower power threshold for nonlinearity and enhanced anharmonicity sensors.

II. THEORETICAL MODEL

We begin with a model considering the nonlinear Kerr effect of the magnon excitation in a YIG sphere which dissipatively interacts with the cavity photons. Here the cavity is directly pumped. This dissipatively coupled nonlinear system is characterized by a Hamiltonian [35,53] (the details shown in Appendix and with reduced units $\hbar \equiv 1$):

$$
\begin{aligned}
H_{\text{tot}} = {} & \omega_c a^+ a + \omega_m b^+ b + K b^+ b b^+ b + i\Gamma(a^+ b + a b^+) \\
& + \Omega_d(a^+ e^{-i\omega t} + a e^{i\omega t}),
\end{aligned} \tag{1}
$$

where a^+ (a) and b^+ (b) correspond to the creation (annihilation) operators of the cavity photons at frequency ω_c and of the Kittel-mode magnons at ω_m, respectively. Here the Kerr effect of magnons term $K b^+ b b^+ b$ originates from magnetocrystalline anisotropy in the YIG material [34], in which K is the Kerr coefficient and is positive in our experiment specifically (see the Appendix). The fourth term of the above equation describes the interaction between the magnon and the cavity photon. In contrast to coherent magnon-photon coupling where the energy is conserved so that the coupling strength is a real number, here the purely imaginary coupling strength ($i\Gamma$) denotes the dissipative coupling. As shown in Ref. [52], dissipative magnon-photon coupling stems from indirect coupling mediated by traveling wave in an open cavity system, where the outgoing boundary conditions result in complex discrete eigenvalues that are described by an effective Hamiltonian that is non-Hermitian [54,57]. The last term in the above equation describes that the cavity is pumped by the oscillating microwave field, with an amplitude Ω_d [58].

By adopting the Heisenberg-Langevin approach [59], the dynamics of the coupled cavity photon-magnon hybrid nonlinear system can be described by the equations:

$$
\frac{da}{dt} = -i(\omega_c - i\kappa)a + \Gamma b - i\Omega_d, \tag{2}
$$

$$
\frac{db}{dt} = -i(\omega_m - i\gamma)b - i(K b b^+ b + K b^+ b b) + \Gamma a. \tag{3}
$$

Under the mean-field approximation [53], the higher-order expectations can be decoupled, so that the nonlinear term $\langle b^+ b b \rangle$ and $\langle b b^+ b \rangle$ can be simplified as $|b|^2 b$, then the dynamics of the dissipatively coupled magnon-photon system follows as

$$
\frac{da}{dt} = -i(\omega_c - i\kappa)a + \Gamma b - i\Omega_d, \tag{4}
$$

$$
\frac{db}{dt} = -i(\omega_m + 2K|b|^2 - i\gamma)b + \Gamma a, \tag{5}
$$

where $\kappa = \kappa_i + \kappa_e$ is the total damping of the cavity mode, with κ_i (κ_e) being the intrinsic (external) damping of the cavity mode. γ is the damping rate of the Kittel mode. Suppose the photon and magnon mode have time dependence of $e^{-i\omega t}$, then Eqs. (4) and (5) can be simplified as

$$
(\omega - \omega_c + i\kappa)a - i\Gamma b = \Omega_d, \tag{6}
$$

$$
(\omega - \omega_m - 2K|b|^2 + i\gamma)b = i\Gamma a. \tag{7}
$$

Equation (6) can be expressed as $a = (i\Gamma b + \Omega_d)/(\omega - \omega_c + i\kappa)$. By substituting such an expression into Eq. (7), we get

$$
|b|[\gamma_m' - i(\delta\omega_m' - 2K|b|^2)] = \frac{\Gamma\Omega_d}{\delta\omega_c + i\kappa}. \tag{8}
$$

Here $\delta\omega_m' = \delta\omega_m + \eta\delta\omega_c$ with $\delta\omega_m = \omega - \omega_m$, $\delta\omega_c = \omega - \omega_c$ denotes effective frequency shift, and

$$
\gamma_m' = \gamma - \eta\kappa, \tag{9}
$$

denotes the effective damping of the magnon for the dissipative coupling system, where the negative sign shows the suppression effect of the magnon damping. We note that for the coherent coupling, the sign is positive representing the enhancement effect of the magnon damping [34,40]. The coefficient $\eta = \Gamma^2/(\delta\omega_c^2 + \kappa^2)$ stands for the transfer efficiency of the excitation power P from the input port into the magnon system, and η is dependent on the dissipative coupling strength Γ, the frequency detuning $\delta\omega_c$, and the total damping κ of the cavity.

Taking the squared modulus of Eq. (8) and defining $\Delta_m \equiv 2K|b|^2$, which is the shift of the magnon frequency [39], we have

$$
\Delta_m\left[\gamma_m'^2 + (\delta\omega_m' - \Delta_m)^2\right] = 2\eta K\Omega_d^2. \tag{10}
$$

Equation (10) has a similar form to the uncoupled Duffing oscillator [3], except that γ_m' and $\delta\omega_m'$ are the effective damping and frequency shift of the magnon, respectively, which result from dissipative coupling with the cavity photon. The right term of Eq. (10) denotes the effective drive field of the magnon via dissipative interaction with the cavity photon as the field directly pumps the cavity rather than the YIG sphere.

A. Bistability and the transition point

Equation (10) describes an oscillator with cubic nonlinearity, called the Duffing equation. As for this equation, there are three real roots for a finite range of frequencies when Ω_d exceeds a specific value called the critical field Ω_t. Among the three roots, one is unstable and the other two are stable, called bistability, which is a signature of the anharmonic oscillator. We will focus on the two boundaries (hereafter termed as top border and bottom border) between which bistability occurs. As there are abrupt transitions between two stable states at top and bottom borders, the transition points of bistability are determined by the condition $d\Omega_d/d\Delta_m = 0$, i.e.,

$$3\Delta_m^2 - 4\delta\omega_m'\Delta_m + \delta\omega_m'^2 + \gamma_m'^2 = 0. \tag{11}$$

According to the root discriminant of the quadratic equation, when $4\delta\omega_m'^2 - 12\gamma_m'^2 = 0$, i.e.,

$$\delta\omega_m' = -\sqrt{3}\gamma_m', \tag{12}$$

there is only one root of Eq. (11), which corresponds to the critical condition of bistable behavior.

When $4\delta\omega_m'^2 - 12\gamma_m'^2 > 0$, there are two real roots which correspond to the top border and bottom border of the bistability. By adopting the approximation $\sqrt{3}\gamma_m' \ll \delta\omega_m'$ to solve Eq. (11), then the top border satisfies

$$\delta\omega_m = 3\sqrt[3]{\frac{\eta K S^2 P}{2}} - \eta\delta\omega_c \text{ (top)}, \tag{13}$$

and the bottom border satisfies

$$\delta\omega_m = \frac{2\eta K S^2 P}{(\gamma - \eta\kappa)^2} - \eta\delta\omega_c \text{ (bottom)}, \tag{14}$$

where $\Omega_d = S\sqrt{P}$, with S describing the conversion efficiency from input power P to the field Ω_d driving the cavity resonance mode. The magnitude of S depends on the frequency, phenomenologically introduced external loss of the cavity field, and the loss in the cable which connects the device. Based on Eqs. (13) and (14), we can come to conclusions that both the top border and bottom border have input power dependence, with the top border satisfying $\delta\omega_m \propto P^{1/3}$ compared with bottom border satisfying $\delta\omega_m \propto P$. These dependencies are different from those of coherently coupled anharmonic oscillators [40], where the top border has $\delta\omega_m \propto P$ dependence and the bottom border $\delta\omega_m \propto P^{1/3}$ dependence. The difference arises from that the magnon shifts to higher frequencies with negative Kerr coefficient K while that of our work shifts to lower frequencies with positive Kerr coefficient. In fact, the two cases can be unified where the border with a large frequency shift has a P dependence and the border with a small frequency shift has a $P^{1/3}$ dependence.

The above discussion is based on tuning the magnetic field to obtain bistability, called field bistability, and its transition point has power dependence. On the other hand, we can adjust input power to obtain bistability, called power bistability, and its transition point has magnetic field dependence. According to Eqs. (13) and (14), we can get borders of power bistability by regarding magnetic field H as an independent variable,

$$P = \frac{2(\delta\omega_m + \eta\delta\omega_c)^3}{27\eta K S^2} \text{ (top)}, \tag{15}$$

$$P = \frac{(\delta\omega_m + \eta\delta\omega_c)(\gamma - \eta\kappa^2)}{2\eta K S^2} \text{ (bottom)}. \tag{16}$$

As the magnon resonance detuning $\delta\omega_m = \gamma_0\delta H$ with definition $\delta H = H - H_r$ (H_r is the resonant magnetic field and γ_0 is gyromagnetic ratio), the top and bottom border of power bistability have respective $|\delta H|^3$ and $|\delta H|$ dependence when up-sweeping and down-sweeping power as shown in Eqs. (15) and (16), respectively.

B. Critical condition of bistability

When Eq. (11) has only one real solution, the bistability vanishes because the two transition points collapse to one point. The critical driving field of the cavity corresponds to the threshold beyond which the bistability appears. Thus, by substituting the critical condition of bistability shown in Eq. (12) and the only solution $\Delta_m = 2/3\delta\omega_m$ into Eq. (10), the critical field Ω_t (critical power P_t) of field bistability is obtained:

$$\Omega_t^2 = \frac{4\sqrt{3}}{9K}\frac{\gamma_m'^3}{\eta}, \tag{17a}$$

$$P_t = \frac{4\sqrt{3}}{9K S^2}\frac{\gamma_m'^3}{\eta}. \tag{17b}$$

These equations imply that the threshold has cubic dependence on the effective damping of magnon γ_m', which is similar to that of coherently coupled nonlinear system [40]. The threshold of nonlinearity for the hybrid system have similar dependence with that of uncoupled ferrimagnetic resonance which has cubic dependence on the damping of magnon (see Table I). Next, we compare the threshold value for the dissipatively coupled system with that of the coherently coupled system. For this purpose, the threshold for a generic two-mode system involving both coherent and dissipative coupling is generated by substituting $\gamma_m' = \gamma + \eta\kappa$ with $\eta = (g + i\Gamma)^2/(\delta\omega_c^2 + \kappa^2)$ into Eqs. (17a) and (17b) where g is the coherent coupling strength. Supposing scenarios $\Gamma = 0$ and $g = 0$, we will get the threshold for coherently coupled and dissipatively coupled systems, respectively. By comparing the thresholds in relation to the nature of coupling (setting $\delta\omega_c = 0$), we have [56]

$$\frac{(\Omega_t^d)^2}{(\Omega_t^c)^2} = \frac{P_t^d}{P_t^c} = \frac{g^2}{\Gamma^2}\left|\frac{1 - \Gamma^2/\kappa\gamma}{1 + g^2/\kappa\gamma}\right|^3, \tag{18}$$

where we have assumed that the two kinds of coupling systems have the same damping coefficient and Ω_t^d (P_t^d), Ω_t^c (P_t^c) denote the critical field (power) of bistability for dissipative and coherent coupling respectively.

Notably, the expression of Eq. (18) is always less than 1 for nonzero Γ and g, revealing a consistently lower threshold in the dissipatively coupled system than that in the coherently coupled system [56]. In order to make a fair comparison, we assume identical magnitudes of coupling strength, i.e., $\Gamma/2\pi = g/2\pi = 21$ MHz. Then, by substituting the value of $\gamma/2\pi = 5.1$ MHz and $\kappa/2\pi = 126$ MHz into Eq. (18), the

TABLE I. Thresholds of the ferrimagnetic materials in the coupled and uncoupled scenarios.

Sample	Threshold	Effective damping[a]
YIG sphere [60]	$\gamma_0^2 h_t^2 = \frac{8\sqrt{3}}{9\chi}\gamma^3 \propto \gamma^{3}$[b]	$\gamma = \gamma_0 \Delta H$[c]
Py film [6]	$\gamma_0^2 h_t^2 = \frac{16\sqrt{3}}{9\gamma_0 M_s}\gamma^3 \propto \gamma^3$	$\gamma = \gamma_0 \Delta H$
YIG (Coh.)[d] [40]	$\Omega_t^2 = \frac{4\sqrt{3}}{9K\eta}\gamma_m'^{3} \propto \gamma_m'^{3}$	$\gamma_m' = \gamma + \eta\kappa$
YIG (Dis.)[e]	$\Omega_t^2 = \frac{4\sqrt{3}}{9K\eta}\gamma_m'^{3} \propto \gamma_m'^{3}$	$\gamma_m' = \gamma - \eta\kappa$

[a]Effective damping of magnon of each system.

[b]Here h_t is the critical drive magnetic field and χ is related to crystalline anisotropy [60].

[c]ΔH is the linewidth of the ferromagnetic resonance.

[d]YIG sphere is placed in a microwave cavity, and they interact coherently.

[e]YIG sphere is placed in a microwave cavity, and they interact dissipatively.

dissipative-coherent threshold ratio becomes a finite value of 0.0064, implying that the dissipative coupling may lead to very low power threshold of the bistability. Such a low threshold arises intrinsically from the suppression of the magnon damping on-resonance [see Eq. (9)] and the cubic dependence of the threshold on the effective magnon damping [indicated by Eqs. (17a) and (17b)].

On the other hand, we can obtain the requirement to observe the power bistability. The only one root of Eq. (11) described by Eq. (12) corresponds to the critical magnetic field to generate power bistability. Combining the relation $\delta\omega_m = \gamma_0 \delta H$ and Eq. (12), the critical magnetic field is given by

$$\delta H = \frac{1}{\gamma_0}[-\eta\delta\omega_c - \sqrt{3}(\gamma - \eta\kappa)]. \quad (19)$$

Compared with the critical magnetic field condition $H - H_r = \sqrt{3}\gamma/\gamma_0$ of uncoupled magnetic systems [6], the extra term of the magnetic field shift $-\sqrt{3}\eta\kappa/\gamma_0$ in Eq. (19) results from the effective damping of the magnon resonance near $\omega = \omega_c$ [23]. The factor $-\eta\delta\omega_c/\gamma_0$ represents the additional resonance shift of the magnon which arises from the interaction between magnon and cavity.

C. Transmission spectra with bistability

The bistability can be detected experimentally via microwave transmission spectra of the cavity. In this section, we show the magnon frequency shift Δ_m (due to the Kerr nonlinearity) is observed in the transmission spectra of the cavity. By considering that the cavity mode couples with the input energy from the port, the dynamic equation Eq. (4) can be rewritten as

$$\frac{da}{dt} = -i(\omega_c - i\kappa)a + \Gamma b + \sqrt{\kappa_e}c_{in}, \quad (20)$$

where c_{in} is the input field. From Eq. (7), the amplitude of the cavity field can be derived

$$b = \frac{i\Gamma a}{\omega - \omega_m - \Delta_m + i\gamma}. \quad (21)$$

According to the input-output theory [59], the relation of input-output field can be described as

$$c_{out} - c_{in} = -\sqrt{\kappa_e}a, \quad (22)$$

where c_{out} is the output field. Combining Eqs. (20), (21), and (22), with the definition of transmission coefficient $S_{21} = c_{out}/c_{in}$, we can obtain the transmission coefficient

$$S_{21} = 1 + \frac{\kappa_e}{i(\omega - \omega_c) - \kappa - \Gamma^2/[i(\omega - \omega_m - \Delta_m) - \gamma]}. \quad (23)$$

The transmission of nonlinear dissipatively coupled system in Eq. (23) can be reduced to that of two coupled linear oscillators if we perform the transformation $\omega_m + \Delta_m \to \omega_m$. Here Δ_m is the nonlinear magnon resonance frequency shift which is the solution of the Duffing equation as shown in Eq. (10). The nonlinear effect can be observed through cavity transmission due to the interaction between the cavity photon and magnon.

III. EXPERIMENTAL RESULTS AND DISCUSSION

A. The hybridized cavity-magnon mode in the linear range

The experimental setup is sketched in Fig. 1(a). A polished YIG sphere with 1 mm diameter is placed at the magnetic field node of a Fabry-Perot-like cavity where the traveling wave dominates [48] such that the excited magnon and the cavity photon are dissipatively coupled, and thereby the coherent coupling strength induced by spatial-overlap of resonant mode is neglected here. The cavity is an assembled apparatus with a circular waveguide connecting to coaxial-rectangular adapters [37,40]. The cavity is pumped by a microwave generator, and the transmission is detected by a signal analyzer. The embedded YIG sphere is placed in a static magnetic field H produced by tunable electromagnets at room temperature, which is not depicted in Fig. 1(a).

We first conduct the experiment under linear conditions, using a vector network analyzer to measure the transmission of the cavity with input power below the threshold to create the nonlinear effect, so that the Kerr nonlinear effect is negligible. Our cavity resonance is at $\omega_c/2\pi = 12.8888$ GHz. The resonance frequency of Kittel-mode in our experiments follows the dispersion $\omega_m = \gamma_0(H_r + H_A)$, where $\gamma_0/2\pi = 29.86\mu_0$ GHz/T is the gyromagnetic ratio, $\mu_0 H_A = -6.1$ mT is the anisotropy field, and H_r is the biased static magnetic field at resonance. When the frequency of the Kittel mode is tuned in resonance with the cavity microwave photons, the standard level attraction of the hybridized modes, which is the signature of dissipative coupling, was measured and is shown in Fig. 1(b). On the left side of this level attraction, an additional mode split caused by the high-order spin wave is not of immediate interest for the discussion of dissipatively coupled nonlinear bistable effect. The dispersion of the hybridized cavity mode and magnon mode is shown in Fig. 1(c), where points A and E correspond to far off-resonance condition with $|\omega - \omega_c| \gg 2\Gamma$, point C indicates on-resonance condition with $|\omega - \omega_c| = 0$, and points B and D indicate an intermediate frequency condition with $|\omega - \omega_c| \sim 2\Gamma$. The dissipative coupling strength can be determined by the separated gap at $\omega_m = \omega_c$ in Fig. 1(d), i.e., $\Gamma/2\pi = 21$ MHz. As
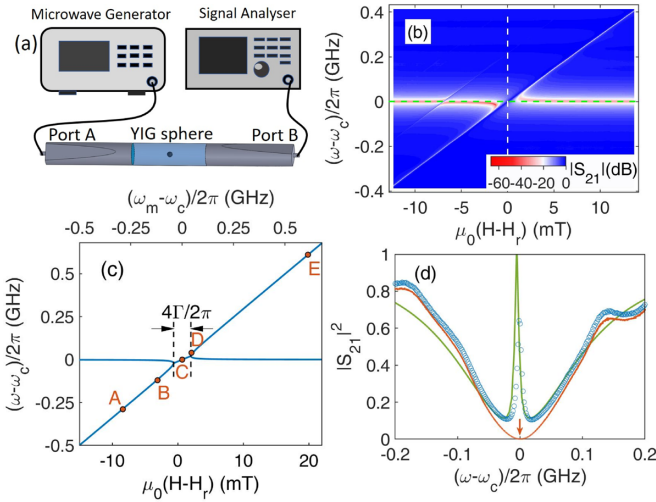
FIG. 1. (a) Illustration of the experimental setup, where a YIG sphere is imbedded in an assembly cavity. Here the YIG is at the node of microwave magnetic field. The cavity is pumped by the microwave generator and the transmission is measured by signal analyzer. (b) Transmission coefficient mapping of the hybridized cavity-magnon system, with level attraction implying dissipative coupling. The white (green) dashed line indicates the vertical (horizontal) cut at the coupling point with $\omega_m = \omega_c$. (c) Dispersion relation of hybridized cavity and magnon mode, where points A and E indicate off-resonance with $|\omega - \omega_c| \gg 2\Gamma$, point C indicates on-resonance with $|\omega - \omega_c| = 0$, and points B and D indicate intermediate frequencies with $|\omega - \omega_c| \sim 2\Gamma$. (d) The fixed magnetic field cut of transmission mapping at the coupling condition $\omega_m = \omega_c$ indicated by white dashed line in (b), with blue symbols for the experimental data and green solid curve for calculated result. And the orange curve denotes the transmission spectra for the bare cavity, with the orange arrow indicating the dip of the transmission spectra which approaches zero.

FIG. 2. $|S_{21}|^2$ versus H with (a) $P = 0.1$ mW and (b) $P = 200$ mW at off-resonant frequency $\omega/2\pi = 12.6000$ GHz. $|S_{21}|^2$ versus H with (c) $P = 0.1$ mW and (d) $P = 200$ mW at on-resonant frequency $\omega/2\pi = 12.8888$ GHz. $|S_{21}|^2$ versus H with (e) $P = 0.1$ mW and (f) $P = 200$ mW at off-resonant frequency $\omega/2\pi = 13.5000$ GHz. Blue (orange) circle symbols are experimental data by up-sweeping (down-sweeping) static magnetic field H. The solid curves are calculated. Dashed green lines with arrows indicate the transition process of bistability and dashed green lines without arrows indicate the unstable state.

seen from Fig. 1(d), the fitting agrees well with the experimental results. The intrinsic and extrinsic linewidth of cavity mode $\kappa_i/2\pi = 2.58$ MHz, $\kappa_e/2\pi = 126$ MHz are obtained by fitting the transmission coefficient spectra when $|\omega_c - \omega_m| \gg 2\Gamma$ where the coupling effect is negligible. Thus, the quality factor of the cavity is 50. The intrinsic and extrinsic dampings of the magnon are 1.6 and 3.5 MHz, respectively. Hence, the total damping of magnon is $\gamma/2\pi = 5.1$ MHz.

B. Field foldover hysteresis loop

In this section, nonlinear effects in our coupled cavity-magnon system for on- and far off-resonance frequencies are measured by sweeping the magnetic field. Here high microwave powers provided by a microwave generator are used to drive the large angle precession of the magnon, while the transmission signal is measured by a signal analyzer, as depicted in Fig. 1(a).

We start our measurements in the linear range by setting the output power of the microwave generator to be 0.1 mW. The transmission was measured at an on-resonance frequency $\omega/2\pi = 12.8888$ GHz indicated by point C in Fig. 1(c), and off-resonance frequencies $\omega/2\pi = 12.6000$ GHz, 13.5000 GHz indicated by points A and E in
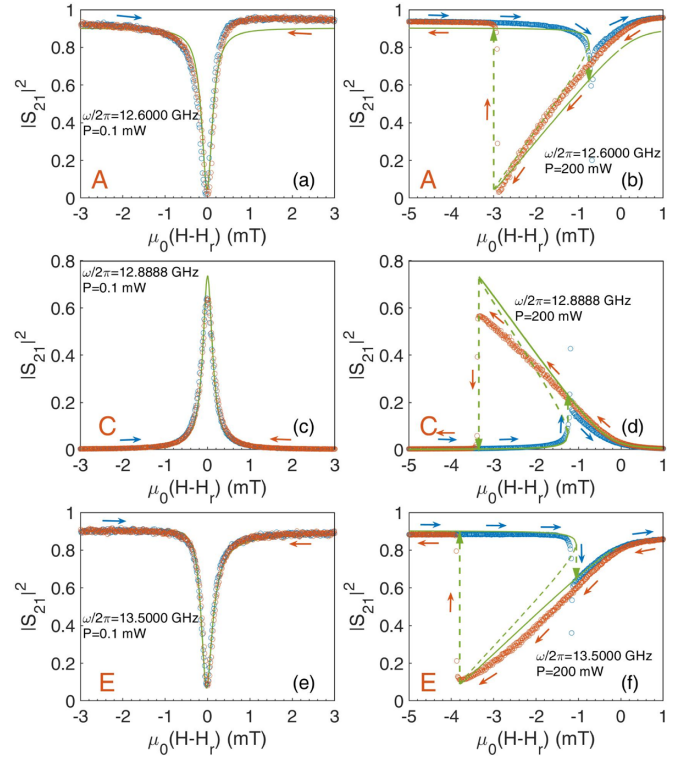
Fig. 1(c), when we perform up-sweeping and down-sweeping magnetic field, as shown in Figs. 2(a), 2(c), and 2(e), respectively. At conditions $\omega/2\pi = 12.6000$ GHz and $\omega/2\pi = 13.5000$ GHz, where the magnon mode is dominant, the spectra show a minimum transmission at the resonance condition $H = H_r$ because of strong absorption due to the magnon excitation as shown in Figs. 2(a) and 2(e). In contrast, the spectrum shows a maximum transmission at condition $\omega = \omega_c$ as shown in Fig. 2(c). Since the extrinsic damping of the cavity is quite large (up to 126 MHz), the overall quality factor of the bare cavity is low ($Q = 50$). Due to the trade-off between the quality factor of the cavity and the resonance intensity of the isolated cavity mode [61], the bare cavity mode reaches a high resonance intensity as the cavity has low quality factor here. The high resonance intensity has signature that the energy is strongly absorbed by the cavity, and thereby the bare cavity transmission approaches zero when $\omega = \omega_c$ as indicated by orange arrow in Fig. 1(d). Such a low resonant transmission will produce a flat background when sweeping the static magnetic field with a fixed microwave frequency up to the resonant cavity frequency, i.e., $\omega = \omega_c$ as shown in Fig. 2(c). When the cavity mode dissipatively couples to a YIG magnon mode at $\omega_m = \omega_c$, the hybrid system

TABLE II. Direction of hysteresis.

	Peak	Dip
$K > 0$	Counterclockwise	Clockwise
$K < 0$	Clockwise	Counterclockwise

will result in a maximum transmission signal at $H = H_r$ [see Fig. 2(c)]. Otherwise, there are only flat transmission spectra approaching zero in Fig. 2(c), which indicates the resonant cavity transmission when sweeping the static magnetic field. As seen by the green dashed cut-line in Fig. 1(b), we can also conclude that the transmission peak arises from the interaction between the cavity and magnon mode.

In order to study the nonlinear effect, we increase power above the threshold. By up- and down-sweeping the magnetic field, we observe that two abrupt jumps of transmission spectra occur at different static magnetic field biases H, corresponding to abrupt transitions between these two stable states. In the range of the transition, a hysteresis loop is clearly seen in the up- and down-sweeping traces of transmission spectra shown in Figs. 2(b), 2(d), and 2(f). This behavior can be explained by Eq. (10), which predicts the behavior of bistability and transitions between the two stable states when the power is above the threshold. The hysteresis loop becomes more evident with the increasing power, because the transition points will depart from each other as microwave power increases, as shown in Figs. 4(a)–4(e).

The bistability of off- and on-resonance have distinctly different behaviors in our magnon-cavity system. When the system is off-resonance, i.e., $|\omega - \omega_c| \gg 2\Gamma$, the field hysteresis loops [Figs. 2(b) and 2(f)] are clockwise when considering the up- and down-sweeping direction of the static magnetic field. In contrast, when the system is on-resonance, i.e., at $\omega = \omega_c$, the field hysteresis loop in Fig. 2(d) is counterclockwise. This behavior is quite different from the bistability of coherently coupled magnon-photon system as measured in Ref. [40]. The work in Ref. [40] demonstrated that when $K < 0$ there is clockwise hysteresis for on-resonance (with peak background) and anticlockwise hysteresis for off-resonance (with dip background).

The direction of hysteresis depends on the sign of K and the background shape of the resonance. For any nonlinear mode with a Lorentzian dip or peak resonance that is excited with high power, the trace of the transmission spectrum will jump at the last transition point along the sweeping direction because of the hysteresis phenomena. For instance, suppose $K > 0$, the trace of the transmission spectrum with peak background will jump at the right transition point from a low to high amplitude by up-sweeping the magnetic field, while it will jump at the left transition point from a high to low amplitude by down-sweeping the magnetic field. Thus, the hysteresis for $K > 0$ and peak background line shape is counterclockwise. By the same approach, the direction of hysteresis can be summarized in Table II, through which the difference in the direction of hysteresis among our measurement and the work of Refs. [34,40] is well explained.

When $|\omega - \omega_c| \sim 2\Gamma$ indicated by points B and D shown in Fig. 1(c), a different foldover hysteresis loop is seen at
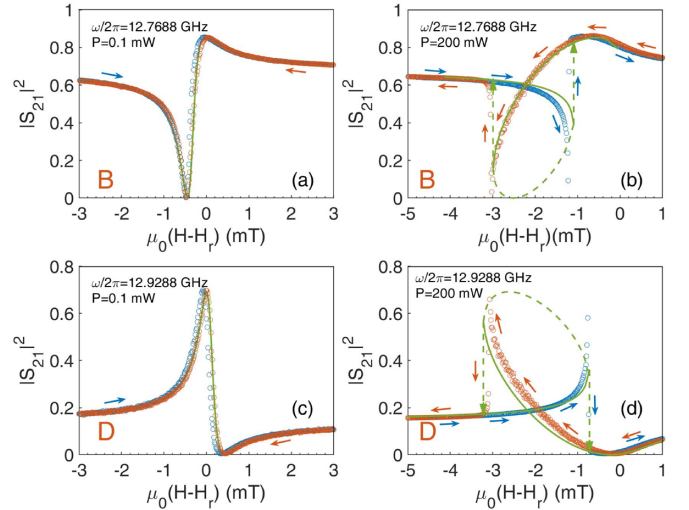

FIG. 3. $|S_{21}|^2$ versus H with (a) $P = 0.1$ mW and (b) $P = 200$ mW at intermediate frequency $\omega/2\pi = 12.7688$ GHz. $|S_{21}|^2$ versus H with (c) $P = 0.1$ mW and (d) $P = 200$ mW at intermediate frequency $\omega/2\pi = 12.9288$ GHz. Blue (orange) circle symbols are experimental data by up-sweeping (down-sweeping) the static magnetic field H. The solid curves are calculated. Dashed green lines with arrow indicate the transition process of bistability and dashed green lines without arrow indicate the unstable state.

intermediate frequencies above and below ω_c. Generally the line shape of transmission spectrum is symmetric when the power is below the nonlinear threshold, for instance, a typical Lorentzian peak characteristic at $\omega = \omega_c$ and a Lorentzian dip $|\omega - \omega_c| \gg 2\Gamma$. However, the line shape of transmission spectrum is asymmetric when the frequency is tuned to the region among $|\omega - \omega_c| \sim 2\Gamma$, shown in Figs. 3(a) and 3(c) with input power 0.1 mW. This asymmetric line shape, similar to that in the coherent scenario [40], is due to Fano-like resonance [62]. However, their polarities are opposite because of different coupling mechanism. As microwave power is increased to 200 mW, in contrast to the general hysteresis loop on- and far off-resonance, a butterfly-like hysteresis loop appears and the polarities of the butterfly-like hysteresis loop are opposite when the microwave frequency is set at intermediate frequencies above and below ω_c as shown in Figs. 3(b) and 3(d). This difference of shape results from the transition direction of bistability. For on- and off-resonance frequency, the direction of two transitions are opposite, where one is from the low to high transmission and another is from the high to low transmission, while, for the intermediate frequencies, the direction of two transitions are identical, i.e., both from high to low transmission or from low to high transmission.

The effective dampings of the magnon are $\gamma'_m/2\pi = 4.50, 3.50, 0.10, 0.15, 5.10$ MHz by fitting the transmission spectra when $P = 0.1$ mW for different frequencies A–E, respectively, which are plotted in Fig. 4(f). The fitted effective damping of the magnon reveals that the damping of the magnon is suppressed on-resonance due to the dissipative interaction between the cavity and the magnon, which is consistent with the result of Ref. [47]. However, this effective magnon damping behavior of the dissipatively
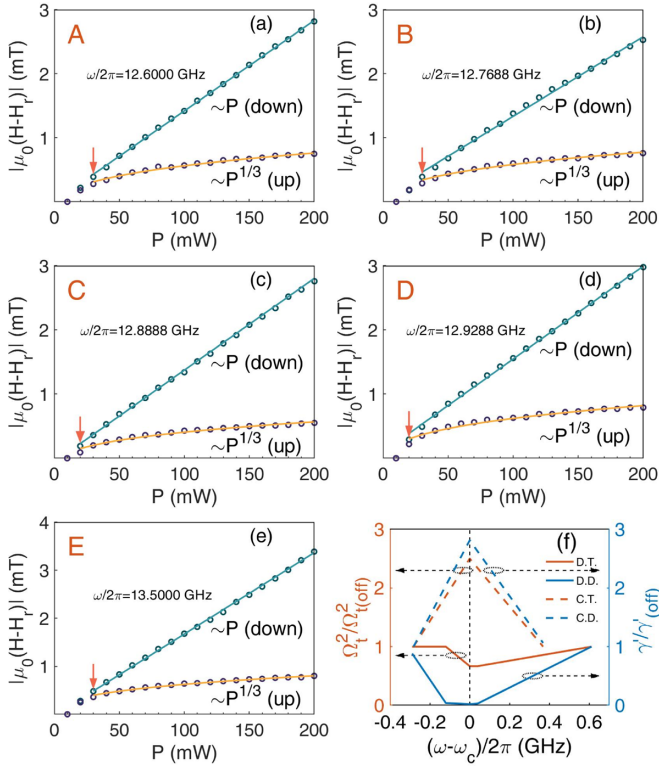
FIG. 4. The jump position of field foldover hysteresis versus P at cavity frequencies (a) $\omega/2\pi = 12.6000$ GHz, (b) $\omega/2\pi = 12.7688$ GHz, (c) $\omega/2\pi = 12.8888$ GHz, (d) $\omega/2\pi = 12.9288$ GHz, and (e) $\omega/2\pi = 13.5000$ GHz. Purple (blue) circle symbols are experimental results of forward (backward) H field sweeping. The yellow and cyan solid curves are fitted using Eqs. (13) and (14) for forward and backward sweeping, respectively. (f) The threshold and effective magnon damping for coherent and dissipative coupling system when off- and on-resonance (indicated by dark dashed line). The threshold and the effective magnon damping for coherent coupling is from Ref. [40]. For simplicity, we consider each threshold and the effective magnon damping relative to those of off-resonance in each system. Here we have utilized the relation $\Omega_t^2/\Omega_{t(\text{off})}^2 = P_t/P_{t(\text{off})}$, where $\Omega_{t(\text{off})}$ and $P_{t(\text{off})}$ are the critical driving field and power off-resonance, respectively. The orange (blue) solid and dashed lines are the relative threshold (the effective magnon damping) for the dissipatively and coherently coupled system with left (right) axis, respectively.

coupled system is distinctly different from that of the coherent scenario in which the effective magnon damping is enhanced as seen in Fig. 4(f). Then, with the damping parameters of the cavity and magnon extracted from the linear process and the solution of Eq. (10), we obtain the fitted parameter $KS^2 = 4.5 \times 10^{-9}, 6.2 \times 10^{-8}, 8.7 \times 10^{-8}, 9.9 \times 10^{-8}, 7.0 \times 10^{-9}$ GHz^3/mW at cavity frequency $\omega/2\pi = 12.6000, 12.7688, 12.8888, 12.9688, 13.5000$ GHz, respectively. (Here K and S cannot be determined individually.) In addition, the fitted transmission spectrum as a function of magnetic field can reproduce the field-sweeping bistability as shown with green line in Figs. 2 and 3. This agreement verifies the validity of our generalized model which describes dissipatively coupled Duffing oscillator and linear oscillator in this quasi-one-dimensional cavity [37].

C. Power dependence of transition and threshold for field foldover hysteresis loop

We have observed that the resonance gradually shifts toward lower H when increasing the microwave power because the Kerr coefficient K is positive (see Appendix). While this is different from the negative Kerr coefficient system where the resonance gradually shifts toward high H [40]. When the power is above the threshold, the bistability appears, and its two transitions will shift depending on the power. Figures 4(a)–4(e) show the jump positions as a function of the microwave power at $\omega/2\pi = 12.6000, 12.7688, 12.8888, 12.9288,$ and 13.5000 GHz, respectively. As predicted by Eqs. (13) and (14), the up-sweeping transition (purple symbols) follows a $P^{1/3}$ dependence (solid line) and the down-sweeping transition (blue symbols) follows a linear P dependence (solid line) with fitted parameters $KS^2 = 4.3 \times 10^{-9}, 5.8 \times 10^{-8}, 8.9 \times 10^{-8}, 8.7 \times 10^{-8}, 6.5 \times 10^{-9}$ GHz^3/mW, respectively. This KS^2 magnitudes determined by fitting the transition points with the power dependence in Eq. (14) is comparable to that fitted by transmission spectrum with Eq. (23). The agreement of KS^2 magnitudes fitted by two different methods is gratifying in view of the error.

The power dependencies are different from those of a coherently coupled nonlinear system, where the down-sweeping jump follows a $P^{1/3}$ dependence and the up-sweeping jump follows a linear P dependence [40]. Because the positive Kerr coeffcient corresponds with $\delta\omega_m < 0$ and negative Kerr coefcient corresponds with $\delta\omega_m > 0$, these opposing frequency shifts will lead to the reversed power dependence of two transition points.

Figures 4(a)–4(e) record the up-sweeping and down-sweeping transition point when increasing power for on- and off-resonance frequencies A–E. We can extract the threshold for each frequency and plot them in Fig. 4(f) for the dissipatively [marked by orange arrows in Figs. 4(a)–4(e)] and coherently (data from Ref. [40]) coupled systems with coupling strength $\Gamma/2\pi = 21$ MHz, $g/2\pi = 18$ MHz, respectively. The results in Fig. 4(f) reveal that the threshold of bistability on-resonance is about 2/3 of those off-resonance in a dissipatively coupled system. This bears stark disparities with a coherently coupled system, where the threshold of the cavity on-resonance is 2.5-fold of that of off-resonance in Ref. [40]. The results imply that the dissipative coupling indeed reduces the threshold despite the fact that our coupled system deviates from anti-PT conditions. In fact, the observed improvement of lower threshold originates from the threshold's cubic dependence on effective magnon damping which remains valid in the dissipative coupling case (see Table I) and the suppressed magnon damping in our dissipative coupling condition [see the extracted effective magnon damping in Fig. 4(f)].

D. Power foldover hysteresis loop and critical magnetic field for power bistability

The hysteresis loops can also be observed by up-sweeping and down-sweeping power at fixed ω and H as shown in Figs. 5(a)–5(e), where we set the biasing magnetic field δH to be $-0.80, -1.04, -0.54, -0.64, -0.76$ mT at cavity frequency $\omega/2\pi = 12.6000, 2.7688, 12.8888, 12.9288,$
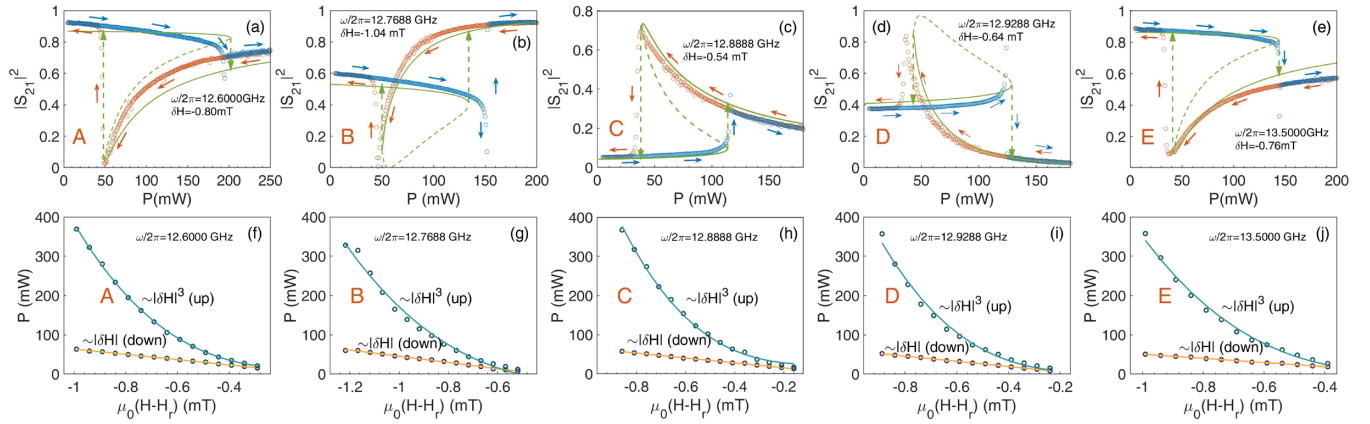
FIG. 5. The power foldover hysteresis with fixed static magnetic field at cavity frequencies (a) $\omega/2\pi = 12.6000\,\text{GHz}$, (b) $\omega/2\pi = 12.7688\,\text{GHz}$, (c) $\omega/2\pi = 12.8888\,\text{GHz}$, (d) $\omega/2\pi = 12.9288\,\text{GHz}$, and (e) $\omega/2\pi = 13.5000\,\text{GHz}$. The recorded power foldover hysteresis transition points versus magnetic field detuning $H - H_r$ at cavity frequencies (f) $\omega/2\pi = 12.6000\,\text{GHz}$, (g) $\omega/2\pi = 12.7688\,\text{GHz}$, (h) $\omega/2\pi = 12.8888\,\text{GHz}$, (i) $\omega/2\pi = 12.9288\,\text{GHz}$, and (j) $\omega/2\pi = 13.5000\,\text{GHz}$.

13.5000 GHz, respectively. In contrast to the case of $K < 0$ with opposite direction for power and field hysteresis [40], here for $K > 0$, they have identical direction at each frequency A–E as shown in Figs. 2(b), 2(d), 2(f), 3(b), 3(d), and 5(a)–5(e).

Figures 5(f)–5(j) show that the transition points of power bistability have $|\delta H|^3$ and $|\delta H|$ dependence for up-sweeping and down-sweeping power, respectively, which agree with the theoretical prediction of Eqs. (15) and (16). As seen in Figs. 5(f)–5(j), the two transition points depart from each other, and the area of power hysteresis loops becomes larger when the bias magnetic field is tuned to be away from H_r and vice versa. At a critical magnetic field H_c, the power hysteresis loops disappear. This phenomenon can be explained by Eq. (19), which implies the requirement of producing power hysteresis loops is that the biasing magnetic field should be below the critical magnetic field at each frequency A–E.

IV. CONCLUSIONS

To summarize, we have observed both the field and power bistability of the dissipatively coupled cavity-magnon system. A theoretical model is studied in which a Duffing and linear oscillator are dissipatively coupled to explain the bistable behaviors. Such a dissipatively coupled hybridized system results in distinctly different bistable behaviors, like butterfly-like, clockwise, and counterclockwise hysteresis which are visualized through transmission spectra. For the field bistability, the transition points show $P^{1/3}$ and P respective dependence when up-sweeping and down-sweeping the magnetic field. Correspondingly, for the power bistability, the transition points show $|\delta H|^3$ and $|\delta H|$ dependence when up-sweeping and down-sweeping power, respectively. Meanwhile, the critical condition required for observing field and power bistability is obtained. With the suppressed magnon damping and therefore lowered threshold for bistability, our system may lay the foundation for wide applications of very low power nonlinearity devices. Indeed, when dissipative coupling dominates between a cavity photon and magnon instead of coherent coupling, it may bring interesting applications

such as low threshold nonlinearity being applicable for magnetic memory and logic gate, and so on, e.g., in Ref. [10]. Besides, benefiting from flexible tunability with, e.g., the magnon frequency, the interaction strength between cavity and magnon, the drive power, the bistability of the cavity magnonics system may be potentially applied in emergent applications like memories and switches.

APPENDIX: HAMILTONIAN OF THE COUPLED HYBRID SYSTEM

The cavity-magnon hybrid system shown in Fig. 1(a) includes a small YIG sphere with Kerr nonlinearity which is dissipatively coupled to a Fabry-Perot-like cavity, and the cavity is driven by a microwave field. The Hamiltonian of such a system consists of four parts (setting $\hbar \equiv 1$):

$$H_{\text{tot}} = H_c + H_m + H_I + H_d, \tag{A1}$$

here $H_c = \omega_c \alpha^+ \alpha$ corresponds to the bare Hamiltonian of the cavity mode, with the creation (annihilation) operator α^+ (α) at frequency ω_c.

In our experiment, we apply a uniform static magnetic field $H = H\mathbf{e_z}$ orientating along the z axis, and the YIG sphere has volume V_m. The static magnetic field is used to align the magnetization and tune the frequency of the magnon mode. When Zeeman energy and magnetocrystalline anisotropy energy are

included, the Hamiltonian of the YIG sphere reads:

$$H_m = -\mu_0 \int_{V_m} \mathbf{M} \cdot \mathbf{H} d\tau - \frac{\mu_0}{2} \int_{V_m} \mathbf{M} \cdot \mathbf{H_{an}} d\tau, \quad \text{(A2)}$$

where μ_0 is the vacuum magnetic permeability, $\mathbf{M} = (M_x, M_y, M_z)$ is the macrospin magnetization of the YIG sphere, and $\mathbf{H_{an}}$ is the magnetocrystalline anisotropy field in the YIG crystal. We have neglected the contribution of demagnetization energy of the YIG sphere in Eq. (A2) as it is a constant term [39,63].

For a uniformly magnetized YIG sphere, which is magnetized along z axis with its anisotropy field along z axis in our experiment, the anisotropy field can be written as $\mathbf{H_{an}} = mM_z\mathbf{e_z}$, where m is dependent on the dominant first-order anisotropy constant and the saturation magnetization [64]. Since $H_A < 0$ in our experiment, we can obtain that $m < 0$. Thus, the Hamiltonian of Eq. (A2) turns out to be

$$H_m = -\mu_0 H M_z V_m + \tfrac{1}{2}\mu_0 m M_z^2 V_m. \quad \text{(A3)}$$

Since the relation between macrospin magnetization $\mathbf{M}$ and macrospin operator $\mathbf{S}$ [34,39,65] is

$$\mathbf{M} = -\frac{\gamma_0 \mathbf{S}}{V_m} = -\frac{\gamma_0}{V_m}(S_x, S_y, S_z), \quad \text{(A4)}$$

where γ_0 is the gyromagnetic ratio. By inserting such relation indicated by Eq. (A4) into Eq. (A3), we obtain

$$H_m = -\mu_0 \gamma_0 H S_z - \frac{\mu_0 m \gamma_0^2 S_z^2}{2V_m}. \quad \text{(A5)}$$

The first term of the above equation corresponds to Zeeman energy. The macrospin operators and the magnon operators are related via the Holstein-Primakoff transformation [66]

$$S^+ = \left[\sqrt{(2S - b^+b)}\right]b, \quad \text{(A6)}$$

$$S^- = b^+\left[\sqrt{(2S - b^+b)}\right], \quad \text{(A7)}$$

$$S_z = S - b^+b, \quad \text{(A8)}$$

where S is the total spin number of the YIG sphere, b^+ (b) the creation (annihilation) operator of the magnon at frequency ω_m, and $S^\pm \equiv S_x \pm iS_y$ are the raising and lowering operators of the macrospin. Through inserting Eq. (A8) into Eq. (A5), the Hamiltonian H_m can be written as

$$H_m = \omega_m b^+b + Kb^+bb^+b, \quad \text{(A9)}$$

here $\omega_m = \mu_0\gamma_0 H + \mu_0\gamma_0^2 mS/V_m$ denotes the frequency of the magnon mode and $K = -\mu_0\gamma_0^2 m/(2V_m)$ the Kerr coefficient. Since $m < 0$ for our experiment, the Kerr coefficient K is positive. Notably, the Kerr effect of magnons term Kb^+bb^+b arises from magnetocrystalline anisotropy. The Hamiltonian representing the interaction between the magnon and the cavity mode is

$$H_I = i\Gamma(b^+ + b)(a^+ + a), \quad \text{(A10)}$$

where Γ denotes the dissipative coupling strength between the magnon and the cavity mode. With the rotating-wave approximation, we can neglect the fast oscillating terms [59], and the cavity-magnon interaction Hamiltonian can be reduced as

$$H_I = i\Gamma(b^+a + ba^+). \quad \text{(A11)}$$

The interaction between the cavity photon and the drive field can be expressed as [58]

$$H_d = \Omega_d(a^+ e^{-i\omega t} + ae^{i\omega t}), \quad \text{(A12)}$$

where Ω_d is the amplitude of the driving field. Finally, we have the total Hamiltonian of the nonlinear cavity magnonics system where the cavity and magnon are dissipatively coupled, and the cavity is directly pumped

$$H_{\text{tot}} = \omega_c a^+a + \omega_m b^+b + Kb^+bb^+b + i\Gamma(a^+b + ab^+)$$
$$+ \Omega_d(a^+e^{-i\omega t} + ae^{i\omega t}). \quad \text{(A13)}$$

[1] A. Camara, R. Kaiser, G. Labeyrie, W. J. Firth, G. L. Oppo, G. R. M. Robb, A. S. Arnold, and T. Ackemann, Optical pattern formation with a two-level nonlinearity, Phys. Rev. A **92**, 013820 (2015).

[2] L. Lugiato, F. Prati, and M. Brambilla, *Nonlinear Optical Systems* (Cambridge University Press, Cambridge, 2015)

[3] L. D. Landau and E. M. Lifshitz, *Mechanics* (Pergamon Press, Oxford, 1969)

[4] K. D. McKinstry, C. E. Patton, and M. Kogekar, Low power nonlinear effects in the ferromagnetic resonance of yttrium iron garnet, J. Appl. Phys. **58**, 925 (1985).

[5] Y. S. Gui, A. Wirthmann, N. Mecking, and C.-M. Hu, Direct measurement of nonlinear ferromagnetic damping via the intrinsic foldover effect, Phys. Rev. B **80**, 060402(R) (2009).

[6] Y. S. Gui, A. Wirthmann, and C.-M. Hu, Foldover ferromagnetic resonance and damping in permalloy microstrips, Phys. Rev. B **80**, 184422 (2009).

[7] P. A. Praveen Janantha, B. Kalinikos, and M. Wu, Foldover of nonlinear eigenmodes in magnetic thin film based feedback rings, Phys. Rev. B **95**, 064422 (2017).

[8] H. Gibbs, *Optical Bistability: Controlling Light with Light* (Elsevier, New York, 2012).

[9] C. Thirion, W. Wernsdorfer, and D. Mailly, Switching of magnetization by nonlinear resonance studied in single nanoparticles, Nat. Mater. **2**, 524 (2003).

[10] R.-C. Shen, Y.-P. Wang, J. Li, S.-Y. Zhu, G. S. Agarwal, and J. Q. You, Long-Time Memory and Ternary Logic Gate using A Multistable Cavity Magnonic System, Phys. Rev. Lett. **127**, 183202 (2021).

[11] C. Valagiannopoulos, A. Sarsen, and A. Alù, Angular memory of photonic metasurfaces, IEEE Trans. Antenn. Propag. **69**, 7720 (2021).

[12] A. Abrashuly and C. Valagiannopoulos, Photonic memory with nonlinear plasmonic nanotubes, APL Mater. **9**, 101111 (2021).

[13] C. Valagiannopoulos, Multistability in coupled nonlinear metasurfaces, IEEE Trans. Anten. Prop. **70**, 5534 (2022).

[14] O. R. Bilal, A. Foehr, and C. Daraio, Bistable metamaterial for switching and cascading elastic vibrations, Proc. Natl. Acad. Sci. USA **114**, 4603 (2017).

[15] F. Cottone, H. Vocca, and L. Gammaitoni, Nonlinear Energy Harvesting, Phys. Rev. Lett. **102**, 080601 (2009).

[16] R. L. Harne and K. Wang, A review of the recent research on vibration energy harvesting via bistable systems, Smart Mater. Struct. **22**, 023001 (2013).

[17] Z.-L. Xiang, S. Ashhab, J. Q. You, and F. Nori, Hybrid quantum circuits: Superconducting circuits interacting with other quantum systems, Rev. Mod. Phys. **85**, 623 (2013).

[18] G. Kurizki, P. Bertet, Y. Kubo, K. Mølmer, D. Petrosyan, P. Rabl, and J. Schmiedmayer, Quantum technologies with hybrid systems, Proc. Natl. Acad. Sci. USA **112**, 3866 (2015).

[19] B. Z. Rameshti, S. V. Kusminskiy, J. A. Haigh, K. Usami, D. Lachance-Quirion, Y. Nakamura, C.-M. Hu, H. X. Tang, G. E. Bauer, and Y. M. Blanter, Cavity magnonics, Phys. Rep. **979**, 1 (2022).

[20] H. Huebl, C. W. Zollitsch, J. Lotze, F. Hocke, M. Greifenstein, A. Marx, R. Gross, and S. T. B. Goennenwein, High Cooperativity in Coupled Microwave Resonator Ferrimagnetic Insulator Hybrids, Phys. Rev. Lett. **111**, 127003 (2013).

[21] Y. Tabuchi, S. Ishino, T. Ishikawa, R. Yamazaki, K. Usami, and Y. Nakamura, Hybridizing Ferromagnetic Magnons and Microwave Photons in the Quantum Limit, Phys. Rev. Lett. **113**, 083603 (2014).

[22] X. Zhang, C.-L. Zou, L. Jiang, and H. X. Tang, Strongly Coupled Magnons and Cavity Microwave Photons, Phys. Rev. Lett. **113**, 156401 (2014).

[23] L. Bai, M. Harder, Y. P. Chen, X. Fan, J. Q. Xiao, and C.-M. Hu, Spin Pumping in Electrodynamically Coupled Magnon-Photon Systems, Phys. Rev. Lett. **114**, 227201 (2015).

[24] X. Zhang, C.-L. Zou, N. Zhu, F. Marquardt, L. Jiang, and H. X. Tang, Magnon dark modes and gradient memory, Nat. Commun. **6**, 8914 (2015).

[25] Y. Tabuchi, S. Ishino, A. Noguchi, T. Ishikawa, R. Yamazaki, K. Usami, and Y. Nakamura, Coherent coupling between a ferromagnetic magnon and a superconducting qubit, Science **349**, 405 (2015).

[26] A. V. Chumak, V. I. Vasyuchka, A. A. Serga, and B. Hillebrands, Magnon spintronics, Nat. Phys. **11**, 453 (2015).

[27] X. Zhang, C.-L. Zou, L. Jiang, and H. X. Tang, Cavity magnomechanics, Sci. Adv. **2**, e1501286 (2016).

[28] A. Osada, R. Hisatomi, A. Noguchi, Y. Tabuchi, R. Yamazaki, K. Usami, M. Sadgrove, R. Yalla, M. Nomura, and Y. Nakamura, Cavity Optomagnonics with Spin-Orbit Coupled Photons, Phys. Rev. Lett. **116**, 223601 (2016).

[29] L. Bai, M. Harder, P. Hyde, Z. Zhang, C.-M. Hu, Y. P. Chen, and J. Q. Xiao, Cavity Mediated Manipulation of Distant Spin Currents using a Cavity-Magnon-Polariton, Phys. Rev. Lett. **118**, 217201 (2017).

[30] D. Zhang, X.-Q. Luo, Y.-P. Wang, T.-F. Li, and J. You, Observation of the exceptional point in cavity magnon-polaritons, Nat. Commun. **8**, 1368 (2017).

[31] J. Li, S.-Y. Zhu, and G. S. Agarwal, Magnon-Photon-Phonon Entanglement in Cavity Magnomechanics, Phys. Rev. Lett. **121**, 203601 (2018).

[32] Z. Zhang, M. O. Scully, and G. S. Agarwal, Quantum entanglement between two magnon modes via kerr nonlinearity driven far from equilibrium, Phys. Rev. Research **1**, 023021 (2019).

[33] J. M. P. Nair and G. S. Agarwal, Deterministic quantum entanglement between macroscopic ferrite samples, Appl. Phys. Lett. **117**, 084001 (2020).

[34] Y.-P. Wang, G.-Q. Zhang, D. Zhang, T.-F. Li, C.-M. Hu, and J. Q. You, Bistability of Cavity Magnon Polaritons, Phys. Rev. Lett. **120**, 057202 (2018).

[35] J. M. P. Nair, Z. Zhang, M. O. Scully, and G. S. Agarwal, Nonlinear spin currents, Phys. Rev. B **102**, 104415 (2020).

[36] Y. Cao, P. Yan, H. Huebl, S. T. B. Goennenwein, and G. E. W. Bauer, Exchange magnon-polaritons in microwave cavities, Phys. Rev. B **91**, 094423 (2015).

[37] B. M. Yao, Y. S. Gui, Y. Xiao, H. Guo, X. S. Chen, W. Lu, C. L. Chien, and C.-M. Hu, Theory and experiment on cavity magnon-polariton in the one-dimensional configuration, Phys. Rev. B **92**, 184407 (2015).

[38] P. Hyde, L. Bai, M. Harder, C. Dyck, and C.-M. Hu, Linking magnon-cavity strong coupling to magnon-polaritons through effective permeability, Phys. Rev. B **95**, 094416 (2017).

[39] Y.-P. Wang, G.-Q. Zhang, D. Zhang, X.-Q. Luo, W. Xiong, S.-P. Wang, T.-F. Li, C.-M. Hu, and J. Q. You, Magnon kerr effect in a strongly coupled cavity-magnon system, Phys. Rev. B **94**, 224410 (2016).

[40] P. Hyde, B. M. Yao, Y. S. Gui, G.-Q. Zhang, J. Q. You, and C.-M. Hu, Direct measurement of foldover in cavity magnon-polariton systems, Phys. Rev. B **98**, 174423 (2018).

[41] R. Hisatomi, A. Osada, Y. Tabuchi, T. Ishikawa, A. Noguchi, R. Yamazaki, K. Usami, and Y. Nakamura, Bidirectional conversion between microwave and light via ferromagnetic magnons, Phys. Rev. B **93**, 174427 (2016).

[42] V. L. Grigoryan, K. Shen, and K. Xia, Synchronized spin-photon coupling in a microwave cavity, Phys. Rev. B **98**, 024406 (2018).

[43] M. Harder, L. Bai, P. Hyde, and C.-M. Hu, Topological properties of a coupled spin-photon system induced by damping, Phys. Rev. B **95**, 214411 (2017).

[44] B. Wang, Z.-X. Liu, C. Kong, H. Xiong, and Y. Wu, Magnon-induced transparency and amplification in pt-symmetric cavity-magnon system, Opt. Express **26**, 20248 (2018).

[45] Y. K. Fetisov, C. E. Patton, and V. T. Synogach, Nonlinear ferromagnetic resonance and foldover in yttrium iron garnet thin films-inadequacy of the classical model, IEEE Trans. Magn. **35**, 4511 (1999).

[46] T. Gerrits, P. Krivosik, M. L. Schneider, C. E. Patton, and T. J. Silva, Direct Detection of Nonlinear Ferromagnetic Resonance in Thin Films by the Magneto-Optical Kerr Effect, Phys. Rev. Lett. **98**, 207602 (2007).

[47] B. Yao, T. Yu, X. Zhang, W. Lu, Y. Gui, C.-M. Hu, and Y. M. Blanter, The microscopic origin of magnon-photon level attraction by traveling waves: Theory and experiment, Phys. Rev. B **100**, 214426 (2019).

[48] M. Harder, Y. Yang, B. M. Yao, C. H. Yu, J. W. Rao, Y. S. Gui, R. L. Stamps, and C.-M. Hu, Level Attraction Due to Dissipative Magnon-Photon Coupling, Phys. Rev. Lett. **121**, 137203 (2018).

[49] B. Bhoi, B. Kim, S.-H. Jang, J. Kim, J. Yang, Y.-J. Cho, and S.-K. Kim, Abnormal anticrossing effect in photon-magnon coupling, Phys. Rev. B **99**, 134426 (2019).

[50] Y. Yang, J. M. Rao, Y. S. Gui, B. M. Yao, W. Lu, and C. M. Hu, Control of the Magnon-Photon Level Attraction in a Planar Cavity, Phys. Rev. Appl. **11**, 054023 (2019).

[51] J. W. Rao, C. H. Yu, Y. T. Zhao, Y. S. Gui, X. L. Fan, D. S. Xue, and C.-M. Hu, Level attraction and level repulsion of magnon

coupled with a cavity anti-resonance, New J. Phys. **21**, 065001 (2019).

[52] Y. P. Wang, J. W. Rao, Y. Yang, P. C. Xu, Y. S. Gui, B. M. Yao, J. Q. You, and C. M. Hu, Nonreciprocity and Unidirectional Invisibility in Cavity Magnonics, Phys. Rev. Lett. **123**, 127202 (2019).

[53] J. M. P. Nair, D. Mukhopadhyay, and G. S. Agarwal, Enhanced Sensing of Weak Anharmonicities through Coherences in Dissipatively Coupled Anti-Pt Symmetric Systems, Phys. Rev. Lett. **126**, 180401 (2021).

[54] Y. Ashida, Z. Gong, and M. Ueda, Non-hermitian physics, Adv. Phys. **69**, 249 (2020).

[55] Y. Yang, Y.-P. Wang, J. W. Rao, Y. S. Gui, B. M. Yao, W. Lu, and C.-M. Hu, Unconventional Singularity in Anti-Parity-Time Symmetric Cavity Magnonics, Phys. Rev. Lett. **125**, 147202 (2020).

[56] J. M. P. Nair, D. Mukhopadhyay, and G. S. Agarwal, Ultralow threshold bistability and generation of long-lived mode in a dissipatively coupled nonlinear system: Application to magnonics, Phys. Rev. B **103**, 224401 (2021).

[57] N. Moiseyev, *Non-Hermitian Quantum Mechanics* (Cambridge University Press, Cambridge, UK, 2011).

[58] G. S. Agarwal and S. Huang, Electromagnetically induced transparency in mechanical effects of light, Phys. Rev. A **81**, 041803(R) (2010).

[59] D. F. Walls and G. J. Milburn, *Quantum Optics* (Springer, Berlin, 2008).

[60] P. Gottlieb, Nonlinear effects of crystalline anisotropy on ferrimagnetic resonance, J. Appl. Phys. **31**, 2059 (1960).

[61] L. Cong, M. Manjappa, N. Xu, I. Al-Naib, W. Zhang, and R. Singh, Fano resonances in terahertz metasurfaces: a figure of merit optimization, Adv. Opt. Mater. **3**, 1537 (2015).

[62] U. Fano, Effects of configuration interaction on intensities and phase shifts, Phys. Rev. **124**, 1866 (1961).

[63] S. Blundell, *Magnetism in Condensed Matter*, Oxford Master Series in Condensed Matter Physics (Oxford University Press, Oxford, 2001).

[64] A. Prabhakar and D. D. Stancil, *Spin Waves: Theory and Applications*, Vol. 5 (Springer, Berlin, 2009).

[65] Ö. O. Soykal and M. E. Flatté, Strong Field Interactions Between a Nanomagnet and a Photonic Cavity, Phys. Rev. Lett. **104**, 077202 (2010).

[66] T. Holstein and H. Primakoff, Field dependence of the intrinsic domain magnetization of a ferromagnet, Phys. Rev. **58**, 1098 (1940).